Nuclear Science and Techniques (2025) 36:5
https://doi.org/10.1007/s41365-024-01572-5

Systematic experimental investigation on pressure build-up characteristics of water-jet injection into a molten LBE pool

Hao-Ran Huang[1] · Zi-Jian Deng[1] · Song-Bai Cheng[1,2] · Jia-Yue Chen[1]

Received: 8 November 2023 / Revised: 11 March 2024 / Accepted: 21 April 2024 / Published online: 18 December 2024

Abstract
In the scenario of a steam generator tube rupture accident in a lead-cooled fast reactor, secondary circuit subcooled water under high pressure is injected into an ordinary-pressure primary vessel, where a molten lead-based alloy (typically pure lead or lead–bismuth eutectic (LBE)) is used as the coolant. To clarify the pressure build-up characteristics under water-jet injection, this study conducted several experiments by injecting pressurized water into a molten LBE pool at Sun Yat-sen University. To obtain a further understanding, several new experimental parameters were adopted, including the melt temperature, water subcooling, injection pressure, injection duration, and nozzle diameter. Through detailed analyses, it was found that the pressure and temperature during the water–melt interaction exhibited a consistent variation trend with our previous water-droplet injection mode LBE experiment. Similarly, the existence of a steam explosion was confirmed, which typically results in a much stronger pressure build-up. For the non-explosion cases, increasing the injection pressure, melt-pool temperature, nozzle diameter, and water subcooling promoted pressure build-up in the melt pool. However, a limited enhancement effect was observed when increasing the injection duration, which may be owing to the continually rising pressure in the interaction vessel or the isolation effect of the generated steam cavity. Regardless of whether a steam explosion occurred, the calculated mechanical and kinetic energy conversion efficiencies of the melt were relatively small (not exceeding 4.1% and 0.7%, respectively). Moreover, the range of the conversion efficiency was similar to that of previous water-droplet experiments, although the upper limit of the jet mode was slightly lower.

Keywords Lead-cooled fast reactor · Steam generator tube rupture accident · Pressure build-up characteristics · Experimental study · Pressure water-jet injection

1 Introduction

The lead-cooled fast reactor (LFR) is generally considered among the most promising candidates for Gen IV nuclear systems [1]. In these reactors, lead-based alloys (usually lead or lead–bismuth eutectic (LBE)) are applied as the primary coolant owing to their excellent heat transport capability, high boiling point, and chemical inertness with air and water [2, 3]. Therefore, for a common pool-type LFR, an intermediate heat transport system need not be installed, and the primary pumps and steam generators (SG) can be installed directly in the primary circuit. This significantly simplifies the system structure and improves the heat transfer efficiency [4]. However, extreme operational conditions (e.g., high-temperature, high-pressure difference between the primary and secondary loops and LBE corrosion risks) in such a

This work was supported by Basic and Applied Basic research foundation of Guangdong province (Nos. 2021A1515010343 and 2022A1515011582) and the Science and Technology Program of Guangdong Province (Nos. 2021A0505030026 and 2022A0505050029).

✉ Song-Bai Cheng
chengsongbai@hrbeu.edu.cn

✉ Jia-Yue Chen
chenjiayue@mail.sysu.edu.cn

1 Sino-French Institute of Nuclear Engineering and Technology, Sun Yat-Sen University, Zhuhai 519082, China

2 College of Nuclear Science and Technology, Harbin Engineering University, Harbin 150001, China

configuration considerably increase the possibility of the occurrence of an SG tube rupture (SGTR) accident [5].

Based on previous research, the evolution of a typical LFR SGTR accident can be divided into four stages [6–9]. In Stage I, secondary water is injected into the primary loop from the rupture location owing to the large pressure difference between the two loops. The injection results in a discontinuity in the pressure field in the two-phase mixture region, where water evaporates and expands intensively owing to the rapid decrease in ambient pressure (flash evaporation phenomenon). This generates an instantaneous pressure shock wave that propagates in the molten lead-based alloy pool. Such a pressure wave applies a sudden load to the surrounding structures and even creates new ruptures in the neighboring SG tubes. In Stage II, owing to the instability at the steam-water interface, a mixture of steam and liquid water is broken up and dispersed in the melt pool, forming a multiphase flow configuration. Meanwhile, the expansion of the mixing zone causes the displacement of the lead-based alloy from the outflow zone, which results in sloshing of the melt pool that could potentially cause mechanical damage to the structures in the primary vessel. In Stage III, certain water droplets may be wrapped in a thin vapor layer. Owing to the protection provided by the vapor layer, these water droplets evaporate slowly in the melt pool [9]. However, under certain triggering actions such as pressure waves, the vapor layer can collapse. Thus, long-lived water droplets are fragmented and come into direct contact with the surrounding molten lead-based alloy (i.e., the coolant–coolant interaction (CCI)), which can bring about drastic evaporation or even trigger an intense steam explosion. Finally, in Stage IV, under the effect of buoyancy force, driving force of the pumps, and drag force of the lead-based alloy flow, the steam bubbles can be entrapped and transported toward the core, potentially causing core reactivity disturbances and inhibiting heat exchange. Among these evolution stages, Stages I and III have a potentially greater risk of causing destructive consequences during an LFR SGTR accident [6]; therefore, these two stages have been chosen as the focus of study by many researchers for over a decade.

In recent years, many experimental and numerical studies have concentrated on the scenario of secondary water injection into primary molten lead-based alloys in Stage I, wherein high-pressure subcooled water is injected into a vessel containing molten LBE. In general, these studies can be divided into three categories: mechanistic experiments, large-scale experiments under working conditions, and numerical simulations. In the first category, Sibamoto et al. [10, 11] conducted experimental investigations at the Japan Atomic Energy Agency (JAEA) by injecting water into a molten LBE pool while using high-frame-rate neutron radiography to visualize the interaction between water and LBE. Furthermore, Zhang et al. [12] conducted several experiments at the Chinese Academy of Sciences by injecting air into the water pool to visually simulate water injection into the LBE pool in Stage I. Recently, Cheng et al. [13] performed certain simulant experiments at Sun Yat-sen University (SYSU) by injecting ethanol and water into the FC-40 fluorinert pool. These studies concentrated primarily on the penetration behavior of a water jet in a molten lead-based alloy pool. Regarding large-scale experiments, a study conducted by Ciampichetti et al. [14, 15] at ENEA in Italy, injected high-pressure subcooled water ($6-7\,\mathrm{MPa}$, $130-235\,°\mathrm{C}$) into the LBE pool ($350-400\,°\mathrm{C}$) through a 4-mm nozzle using the LIFUS 5 facility. In their study, pressure and temperature fluctuations during the interaction were studied. In addition, Yu et al. [16] conducted several similar experiments using the LBE SGTR test facility (LEST) at Xi'an Jiaotong University, with a focus on pressure fluctuation and steam cavity migration. Several researchers have conducted numerical studies on this topic. For example, in addition to the experiments at the LIFUS5 and LIFUS5/Mod2 facilities, numerical simulations using the SIMMER-III code were also performed [14, 15, 17] at ENEA based on their experimental conditions. Further, researchers from Shenzhen University conducted numerical investigations to simulate the experiments of Sibamoto et al. [11] and Pesetti et al. [17] using the MC3D code [18]. Iskhakov et al. [7] proposed two approaches for estimating the forces acting on neighboring tubes using one-dimensional (1D) spherical coordinate models under the conditions of the steam generator of the BREST-OD-300 reactor.

Experimental and numerical studies were also conducted for Stage III, that is, a water droplet entrapped within a molten lead-based alloy pool. For example, Cheng et al. [19] conducted an experimental study by delivering several dozen milliliters of water lumps into a molten Bi-Sn-In pool at JAEA. Several studies have focused on the pressure build-up characteristics during Stage III conducted at SYSU using an experimental facility called the pressurization characteristics in melt–coolant interaction (PMCI) [20–23]. This facility has been proven to be capable of rectifying several defects in the JAEA [19, 20, 23]. For example, Zhang et al. [23] conducted several experiments by delivering water lumps to the bottom of a molten Bi-Sn-In alloy pool. Recently, Cheng et al. [21, 22] released water lumps of different volumes and shapes into a molten LBE pool. All three studies have reported a limited pressure build-up when the water volume increases, this is because the isolation effect of the vapor layer at the water–melt interface is the primary cause. These results are consistent with a previous numerical study on the water–melt interaction at JAEA using the SIMMER-III code performed by Cheng et al. [24]. Further, Iskhakov et al. [8] analyzed the steam explosion phenomenon using a model of multiphase thermal detonation and Hugoniot adibats.

However, despite significant efforts, there several defects have been observed in past studies on Stage I. For example, in the studies by Ciampichetti et al. [14, 15] and Yu et al. [16], experiments were conducted under the working conditions of an actual LFR; however, the experimental parameters were limited to a relatively narrow range. In existing mechanistic studies, such as those of Sibamoto et al. [10, 11], Zhang et al. [12], and Cheng et al. [13], more experimental parameters were considered compared to large-scale experiments. Although the interaction behavior between the water jet and molten LBE can be effectively visualized using neutron radiography and transparent simulant materials, it is still difficult to determine the pressure build-up characteristics during the interaction through a two-dimensional (2D) view of the mixing zone in an open interaction vessel connected to the atmosphere. Furthermore, in the studies by Zhang et al. [12] and Cheng et al. [13], certain reliability issues related to the simulant materials in the experiments, such as whether the results obtained can be adopted directly under actual conditions, remain. Therefore, the present knowledge on the interaction mechanism of a water jet with molten LBE during Stage I remains limited, and a clearer investigation by systematic experiments is urgently required.

Focusing on the interaction mechanism in Stage I, there study conducted several new experiments by injecting pressurized water into a molten LBE pool using the PMCI experimental facility at SYSU. To acquire a deeper understanding of the pressure build-up characteristics during Stage I, various experimental parameters, including injection pressure, injection duration, nozzle diameter, and temperature of both liquids, were considered. The remainder of this paper is organized as follows. In Sect. 2, the PMCI facility and the experimental conditions related to all the experimental cases in this study are described in detail. In Sect. 3, the history of both steam explosion and non-explosion cases in the transient state, the influence of experimental parameters on pressure build-up, and the energy conversion efficiency (including the overall mechanical energy efficiency and kinetic energy efficiency of the melt) are analyzed and interpreted in detail. Specifically, to deepen the understanding of the mechanism of water–melt interaction, the experimental results in this study are compared with those of our previous studies focusing on Stage III. The knowledge and experimental data accumulated in this study can be applied to validate numerical models in the future.

2 Experimental details

As mentioned in Sect. 1, the PMCI experimental facility was designed and established based on the original facility at JAEA, and has reduced uncertainties in experiments and enhanced operability compared to its predecessor [19, 20, 23]. Moreover, in contrast to previous studies, this study focused on Stage I instead of Stage III; thus, the water delivery system of the PMCI facility was replaced by a water-jet injection system. Figure 1 presents a schematic of the PMCI facility employed in this study.

The interaction vessel of the PMCI facility is a rigid cylindrical vessel made of 316 L stainless steel with an inner diameter of 250 mm and height of 750 mm, which is capable of resisting instantaneous pressure build-up (up to 40 MPa) during interaction. To measure the transient temperature and pressure at different regions (i.e., the molten LBE pool and cover gas) during the interaction, several K-type thermocouples and dynamic pressure sensors were installed at the corresponding locations, as shown in Fig. 1. Detailed information on these instruments is provided in Table 1. For safety purposes, an outer vessel was used to contain and isolate the interacting vessels.

Before melting, a chemical composition test was performed on the LBE ingots, which showed that the oxidized part was negligible. To maintain the target liquid level in the melt pool during the experiments, the mass of LBE was calculated at room temperature (293 K) before being loaded into the interaction vessel. An inductive electromagnetic heater with a coil wrapped around the outer wall of the interaction vessel (Fig. 1), can produce approximately 40 kW heating power for heating and melting LBE. Before heating, an inert gas was introduced into the interaction vessel to evacuate the air and prevent the oxidation of LBE.

The injection system, which included a stainless-steel container, solenoid valve, and injection tube, was installed on the top cover of the interaction vessel (Fig. 1). A rubber sealing ring was inserted between the top cover and interaction vessel to ensure airtightness during the experiment. Before each run, pure water was added to the stainless-steel container. A resistance heater attached to the outer wall of the container was used to heat the water, and the water temperature was controlled using a digital heating device. When the water temperature reached the set value, it was sustained by the control device in the following steps. During the heating, an inert gas was introduced to pressurize the water in the container. A solenoid valve connected to a release control device was installed below the container to control injection duration. One end of the injection tube was screwed to the solenoid valve, and the other end was a nozzle with different diameters. The tube was inserted into the melt pool (approximately 10 mm) through the top cover of the interaction vessel. After the temperatures of the molten LBE and water reached the desired values, the water jet was released into the molten LBE pool.

To clarify the pressure build-up characteristics during Stage I (i.e., under the scenario of water-jet injection into a molten LBE pool), several experimental parameters, including water temperature (T_w) (or water subcooling

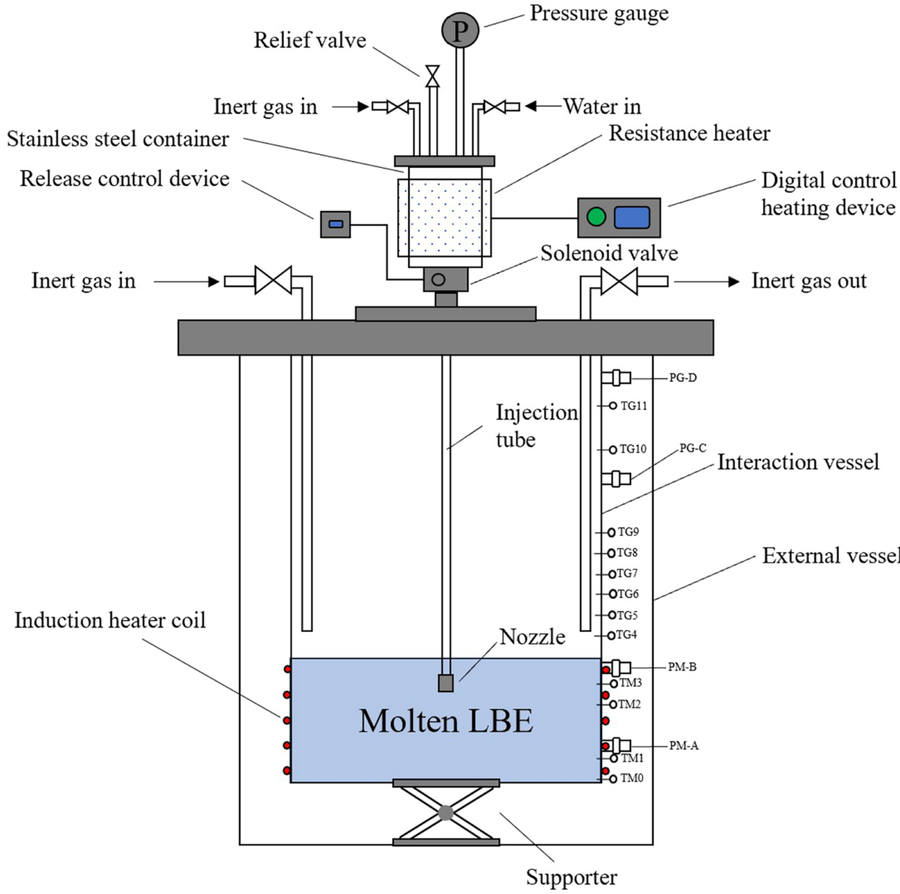

Fig. 1 Schematic of PMCI experimental facility

Table 1 Detailed information of sensors and their descriptions [22, 23]

Sensor	Measuring parameter	Measuring region
PM-A, PM-B	Pressure	Melt pool
PM-C, PM-D		Cover gas
TM0–TM3	Temperature	Melt pool
TG4–TG11		Cover gas

(ΔT_{sub})), injection pressure (P_i), injection duration (T_i), LBE temperature (T_m), and nozzle diameter (d), were considered. Table 2 lists the specific conditions of all experimental cases in this study. In this study, the LBE temperature range was set based on the working conditions of China's CLEAR-I, which uses LBE as the primary coolant. The core inlet and outlet temperatures were 573 K and 673 K, respectively [25]. The water temperature range was set based on the water subcooling in the actual LFRs. In this study, water subcooling ranged as 20–80 K in the experimental pressure range, which is equivalent to the water subcooling range in the design specifications of certain typical LFRs (e.g., CLEAR-I with a designed water subcooling of 80 K) [26].

Furthermore, as mentioned by [27], the boiling mode during the interaction of water with the melt could also have a significant influence on the evaporation rate of water and thus on the pressure build-up characteristics. In previous studies [28–30], a criterion for the boiling mode was proposed from a thermal perspective. During sudden contact between cold and hot liquids, if the instantaneous contact interface temperature T_i is higher than the homogeneous nucleation temperature T_{hn}, then the cold liquid evaporates sufficiently violently to trigger a steam explosion [31]. These two temperatures can be calculated using the following equations [31, 32]:

$$\frac{T_i - T_c}{T_h - T_i} = \left(\frac{K_h \rho_h C_h}{K_c \rho_c C_c}\right)^{1/2}, \tag{1}$$

$$T_{hn} = T_{sat} + \left[0.905 - \left(\frac{T_{sat} + 273}{T_{crit} - 273}\right) + 0.095\left(\frac{T_{sat} + 273}{T_{crit} - 273}\right)^8\right] \times (T_{crit} + 273), \tag{2}$$

Table 2 Specific conditions of experimental cases in this study

Run No.	P_i (MPa)	$T_w(\Delta T_{sub})$ (K)	T_m (K)	t_i (s)	d (mm)	Steam explosion*
1	0.equation	293(80)	573	1	2	N
2			598			N
3			623			N
4			648			N
5			673			N
6			598	2		N
7			623			N
8			648			N
9			598	3		N
10			623			N
11			648			N
12	0.3		598	1		N
13			623			N
14			623	2		N
15	0.35		573	1		N
16			598			N
17			623			N
18			648			N
19			673			Y
20			598	2		N
21			623			N
22			648			N
23			673			Y
24			598	3		N
25	0.4		573	1		N
26			598			N
27			623			N
28			648			N
29			673			N
30			623	2		N
31	0.25	313(60)	623	1		N
32			648			N
33		333(40)	623			N
34			648			N
35		353(20)	623			N
36			648			N
37		293(80)	573		4	N
38			698			N
39			623			N
40			648			N
41			673			N

* Y implies that steam explosion is observed in corresponding run, otherwise noted as N

where K, ρ, and C denote the thermal conductivity, density, and specific heat, respectively. The subscripts 'c' and 'h' denote the cold and hot liquids, respectively. Further, T_{sat} is the saturation temperature of water and T_{crit} is the critical temperature of water (647 K). However, an upper temperature limit exists for this boiling mode. If the instantaneous contact interface temperature T_i is higher than the minimum film boiling temperature T_{mfb}, a stable vapor film is formed at the interface of the water and the melt, which significantly inhibits heat transfer between the two materials.

The minimum film boiling temperature was calculated using the following equation [33]:

$$T_{mfb} = T_{sat} + (101 + 8\Delta T_{sub}), \tag{3}$$

where ΔT_{sub} is the water subcooling. Therefore, if the water–melt temperature combination is in the zone where $T_i > T_{hn}$ and $T_i < T_{mfb}$, a steam explosion might be triggered. Based on this criterion, it is possible to predict the boiling mode for each experimental case, as shown in Fig. 2.

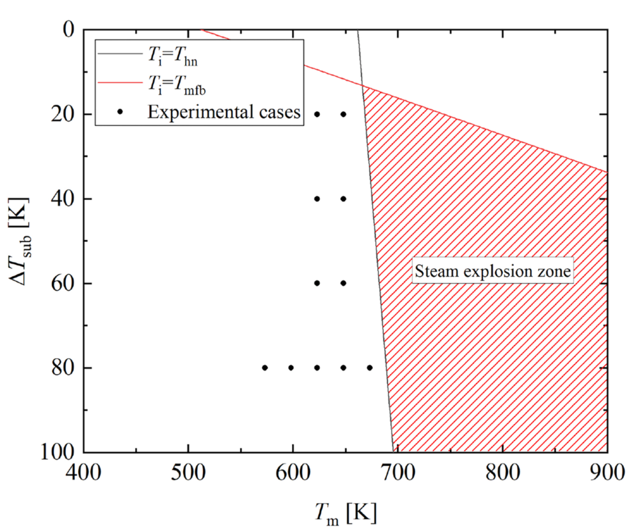

Fig. 2 Boiling mode predicted according to above thermal criterion for each experimental case

3 Experimental analyses and discussion

3.1 Transient behavior of representative cases

Similar to the studies by Cheng et al. [21, 22] that focused on Stage III, two interaction mechanisms (i.e., steam explosion and non-explosion) were observed, and their corresponding conditions are listed in Table 2. Because visualization methods (such as neutron radiography) were not applied in the experiments in this study, the water–melt interaction could not be directly observed. Therefore, pressure history was used to determine the interaction mechanism. Because these two different interaction mechanisms may cause two transient behaviors with evident differences, two representative runs in each category are discussed separately in this section.

Among the cases wherein a steam explosion did not occur, case No. 17 was selected for analysis, and its measured transient temperature and pressure histories are shown in Fig. 3. In the pressure history, it can be clearly observed that after direct contact between the water jet and the melt pool, water evaporated rapidly and created several pressure pulses in the melt pool. This trend was very similar to the transient behavior of the water-droplet mode in previous studies by Cheng et al. [21, 22], wherein a three-phase evolution could be distinguished. In Phase (1), in the water and melt premix, water evaporated and condensed simultaneously, and the pressure increased slightly from the initial constant value. In Phase (2), water evaporated rapidly, leading to a spike in the melt pressure history called the two-phase pressure [19], which was used to characterize the pressure build-up in the melt pool. In Phase (3), the generated steam expanded, that is, the pressure decreased gradually from a maximum value owing to steam condensation.

In this case, the peak value of the two-phase pressure was relatively small (approximately 0.19 MPa), and the duration was quite short (several tens of milliseconds). In addition, because there is still a large space in the interaction vessel, the pressure in the cover gas region increased continuously at a relatively low rate. However, with respect to the temperature history, there was no significant change in temperature in either the melt pool or cover gas region. This is because the melt pool and cover gas regions have a considerably larger scale than the volume of the water jet per run; therefore, the temperature variation in both regions is negligible.

For the steam explosion cases, case No. 19 was selected for analysis, and its measured transient temperature and pressure histories are shown in Fig. 4. A comparison of the pressure histories of the non-explosion cases in Fig. 3 revealed a consistent overall trend despite of their different interaction mechanisms. However, a considerably more intensive two-phase pressure, with a peak value of 0.9 MPa and a duration of several tens of milliseconds, was generated during the water–melt interaction in this case, and the pressure increase rate in the cover gas region was also higher. In addition, because the volume of water injected into the melt pool remained almost unchanged, the temperature variations in the melt pool and cover gas regions remained relatively minor.

3.2 Influence of experimental parameters on pressure build-up characteristics

To quantitatively analyze the influence of the experimental parameters on the pressure build-up characteristics, the method applied in previous studies [19–23, 27] was also used in this study.

During Stage I of SGTR accident, flash evaporation of the water jet occurs, creating a pressure wave in the melt pool that can cause mechanical damage to in-vessel structures. As mentioned in Sect. 3.1, several pressure pulses are generated in the melt pool during the water–melt interaction, among which the first two-phase pressure is the most intensive. Therefore, the impulse I applied to

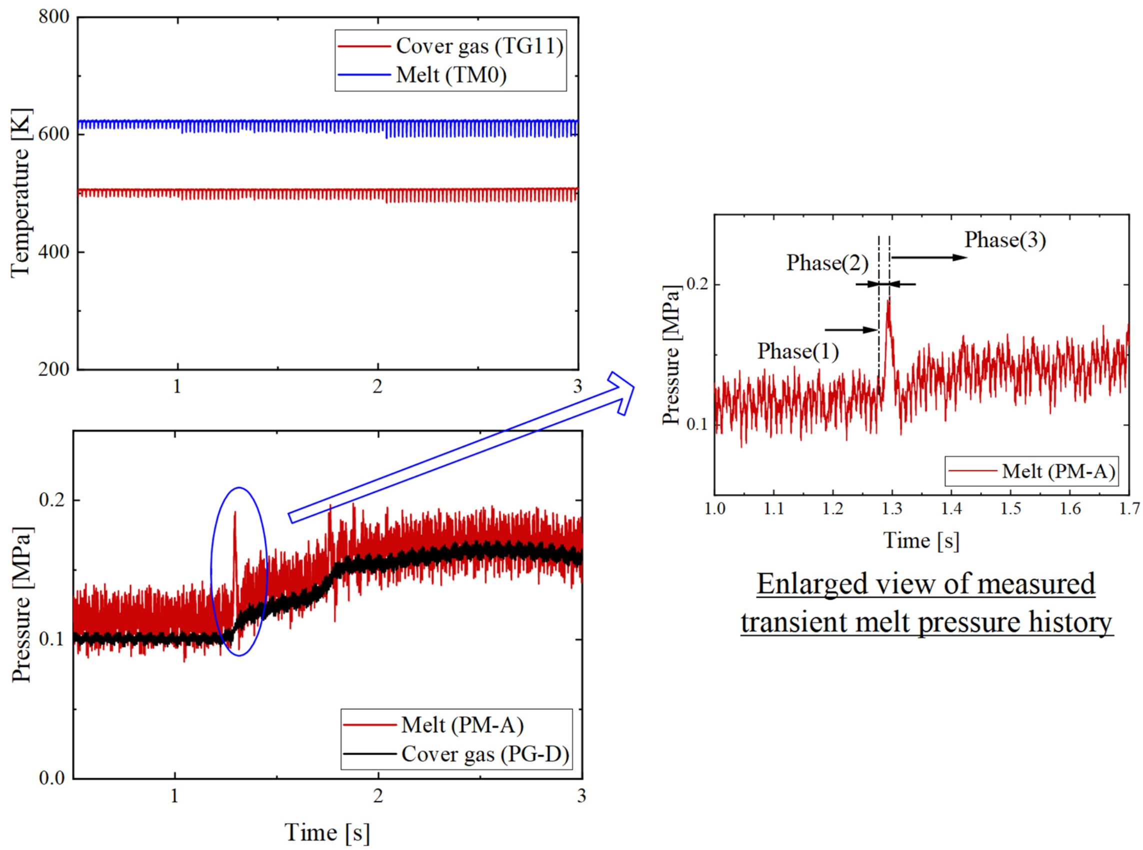

Fig. 3 (Color online) Transient pressure and temperature history of non-explosion case ($P_i = 0.35$ MPa, $T_w = 293$ K, $T_m = 623$ K, $t_i = 1$ s, $d = 2$ mm)

the melt pool by the first two-phase pressure was used to characterize the intensity of the pressure wave in the melt pool:

$$I = A \int P(t)\mathrm{d}t, \tag{4}$$

where A, P, and t represent the cross section of the interaction vessel, pressure, and time, respectively.

According to the original study [19], this method is more appropriate for analysis than the method that uses the peak value. As shown in Figs. 3 and 4, there were many fluctuations in the measured pressure history data, the integration could greatly reduce the influence of noises and represent an overall variation trend.

In this section, the influence of the experimental parameters on the pressure build-up characteristics is discussed. As shown in Table 2, there were only a few experimental cases wherein a steam explosion was observed; thus, the impulse of the steam explosion cases was be calculated in the subsection of each parameter. Instead, the influence of the interaction mechanism was analyzed separately.

3.2.1 LBE temperature

To investigate the influence of the molten LBE temperature on the pressure build-up characteristics, the calculated impulses at different molten LBE temperatures (from 573 K to 673 K) under two injection pressures (0.25 MPa and 0.40 MPa) are shown in Fig. 5. According to Table 2, all the cases involved here were non-explosion cases.

As shown in Fig. 5, despite the difference in injection pressure, increasing melt-pool temperature increased the pressure wave intensity. Theoretically, as the melt-pool temperature increased, the heat transfer between the water jet and molten LBE was promoted, and the water evaporated more violently. Consequently, a more intense pressure wave was generated in the melt pool.

3.2.2 Water subcooling

The influence of water subcooling on the pressure build-up characteristics under melt temperatures of 623 K and 648 K is shown in Fig. 6.

Figure 6 indicates a consistent trend in the influence of water subcooling. As the water subcooling temperature

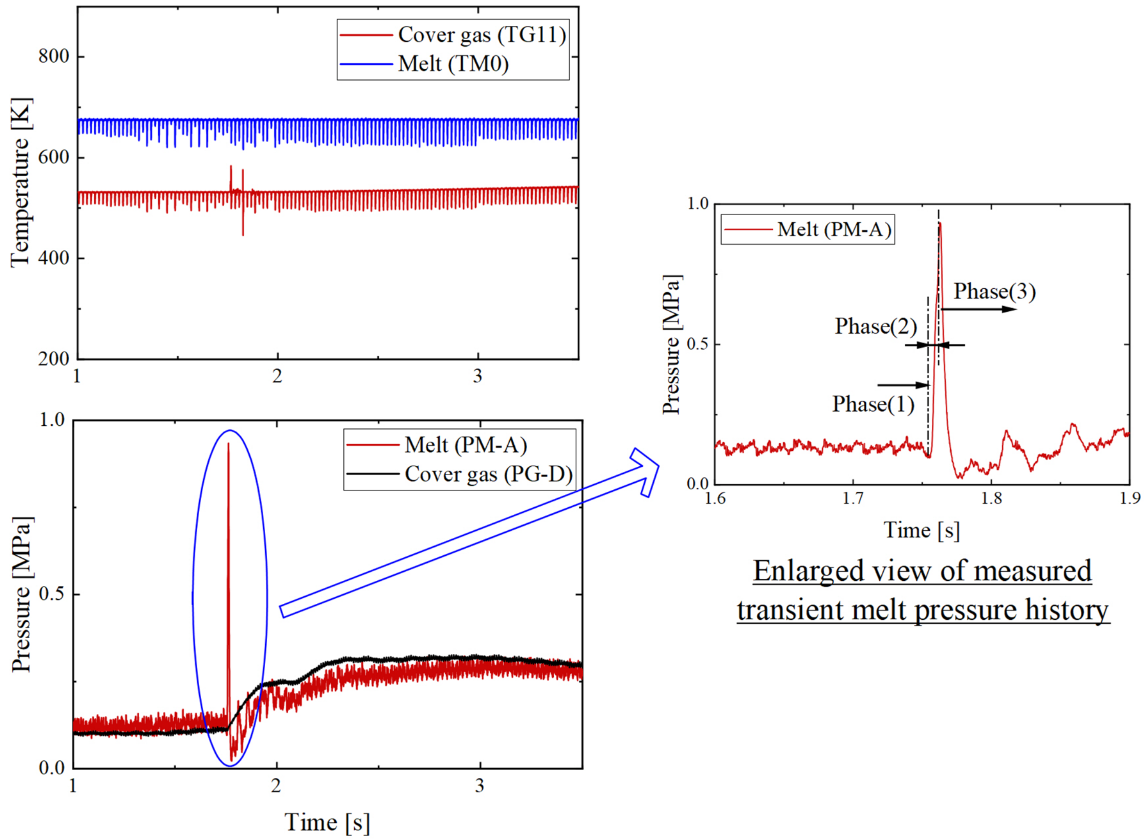

Fig. 4 (Color online) Transient pressure and temperature history of steam explosion case (P_i = 0.35 MPa, T_w = 293 K, T_m = 673 K, t_i = 1 s, d = 2 mm)

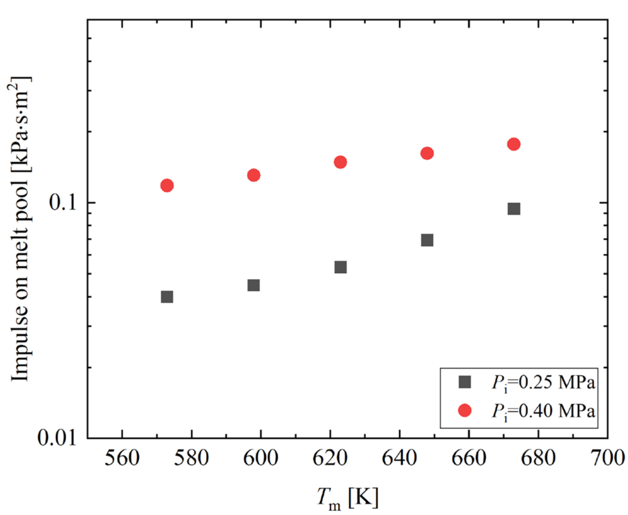

Fig. 5 Influence of molten LBE temperature on pressure build-up characteristics (T_w = 293 K, t_i = 1 s, d = 2 mm)

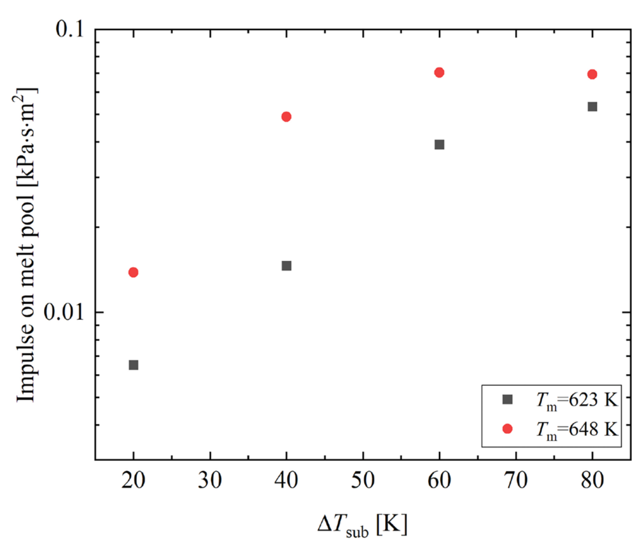

Fig. 6 Influence of water subcooling (P_i = 0.25 MPa, t_i = 1 s, d = 2 mm)

increased (or the water temperature decreased), the pressure wave intensity tended to increase. This influence pattern was completely different from that in previous water-droplet mode studies [20–23], where water subcooling had no significant effect on the pressure wave intensity. In theory, there are two possible factors that could influence heat transfer efficiency and thus pressure wave intensity: the water–melt temperature difference and the boiling mode of water. However, it is noteworthy that the product of water heat capacity and water subcooling was significantly lower than the latent heat of water. Thus, despite the increase in the water–melt temperature difference as the water subcooling increased, the required energy for evaporation did not vary greatly. Therefore, this seems to conflict with the variation in the pressure wave intensity shown in Fig. 6 which is clearly observed to be more significant than the one in Sect. 3.2.1. This suggests that the water–melt temperature difference should not be the major influence factor.

Considering that phase change is involved in the interaction of water and the melt, the boiling mode of water should be the definitive factor. Notably, during the experiment, the cases with water subcooling of 20 K were very mild, whereas blast sounds occurred in the other cases. Referring to Fig. 2, although from the thermal aspect, all the experimental cases were not within the steam explosion zone or the film boiling zone (where $T_i > T_{hn}$ and $T_i > T_{mfb}$), their relative positions to these two zones could explain the phenomenon to a certain extent. In Fig. 2, as the water subcooling decreased, the experimental conditions were closer to the film boiling zone. It is reasonable to presume that under such conditions, film boiling occurs at certain locations on the water–melt interface, and the overall heat transfer is inhibited; thus, a pressure wave with reduced intensity is observed. Compared with previous water-droplet mode studies [20–23], the water jet was more likely to be broken up into many smaller fragmented droplets, thereby introducing a larger water–melt contact area. Consequently, the overall possibility of local boiling mode transformation increased. This enhancement explains why the influence pattern of water subcooling in this study was different from those in previous water-droplet mode studies.

3.2.3 Injection pressure

The influence of the injection pressure on the pressure build-up characteristics is shown in Fig. 7, with melt temperature of 598 K and injection duration of 1 s and melt temperature of 623 K and injection durations of 1 s and 2 s.

Figure 7 shows that, irrespective of injection duration and melt-pool temperature, increasing injection pressure generally leads to enlarged pressure wave in melt pool. Theoretically, the higher the injection pressure, the higher the velocity of the water jet, which implies an increase in the volume of water entering the melt pool per unit time. In addition, an increase in the water jet velocity resulted in greater momentum, and the penetration effect was significantly enhanced. Consequently, these two potential factors increased the contact area of the water and melt and substantially enhanced

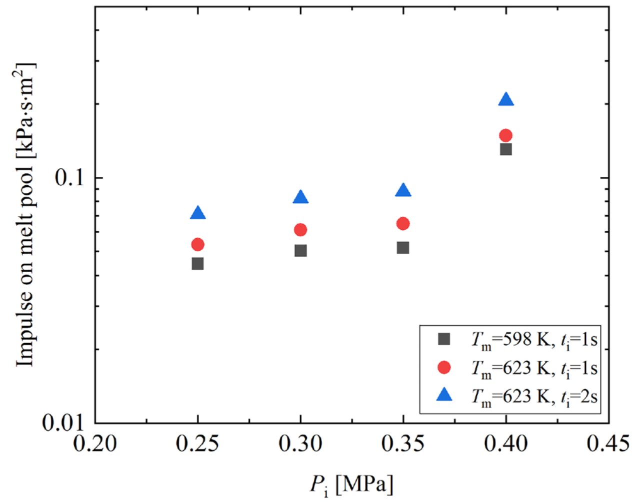

Fig. 7 Influence of injection pressure on pressure build-up characteristics (T_w = 293 K, d = 2 mm)

the heat exchange between the two materials, creating more energetic pressure waves in the melt pool.

Furthermore, as the injection pressure increased from 0.25 MPa to 0.35 MPa, the pressure wave intensity increased at a relatively low rate, whereas the growth rate was considerably higher as the injection pressure reached 0.40 MPa. It seems reasonable to conclude that as the injection pressure reached a certain level, the momentum of the water jet was sufficiently large to resist the buoyancy force effect of the molten LBE. At such injection pressures, the pressure plays a dominant role in penetration, allowing the water jet to arrive at a deeper region of the melt pool, which significantly increases the water–melt contact area. Therefore, a significantly more intense pressure wave was observed at this injection pressure level.

3.2.4 Injection duration

The influence of the injection duration on the pressure build-up characteristics under different melt temperatures (from 598 K to 648 K) and injection pressures (0.25 MPa and 0.35 MPa) is shown in Fig. 8.

As displayed in Fig. 8, as the injection duration increased, the intensity of the pressure wave first increased and then tended to become saturated. This occurred regardless of the differences in melt temperature and injection pressure. Referring to previous studies wherein a water lump was delivered into a melt pool [20–23], a consistent influence pattern of the water volume was observed.

As indicated by Sibamoto et al. [10, 11], in their visualization experiments, when water was injected into a molten LBE pool, a cavity was formed as water evaporated, and water accumulated in the cavity. It is inferred that such a

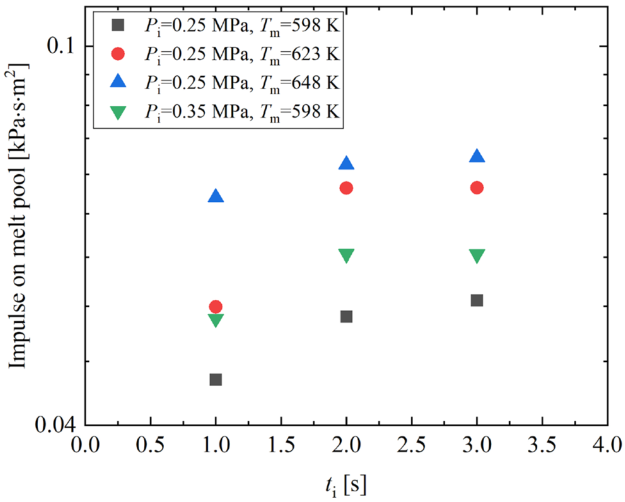

Fig. 8 Influence of injection duration on pressure build-up characteristics ($T_w = 293$ K, $d = 2$ mm)

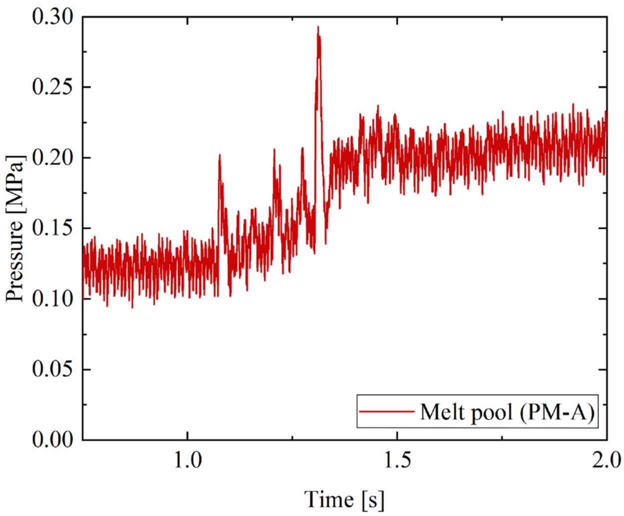

Fig. 9 Melt-pool pressure history of run No. 7 ($P_i = 0.25$ MPa, $T_w = 293$ K, $T_m = 623$ K, $t_i = 2$ s, $d = 2$ mm)

cavity can play a key role in interfering with the direct contact between the water and the melt pool. Thus, it is rational to conclude that the isolation effect of the cavity may result in the saturation of the pressure wave intensity.

Although it was not feasible to directly observe whether a cavity was formed during the injection process in this study, it is still possible to speculate the existence of a cavity. Several experimental cases provide evidence of cavity formation. Figure 9 shows the pressure history of the melt pool in one of these cases. As evident, during the pressure build-up process, multiple two-phase pressures were observed and the last one had the greatest peak value, signifying that water interacted 'in batches' with melt. It is reasonable to presume that the first few relatively weak two-phase pressures were owing to the formation of a cavity, and the last strongest two-phase pressure corresponded to the interaction between the water accumulated in the cavity and the surrounding melt.

However, there is another hypothesis regarding this saturation phenomenon. As mentioned in Sect. 2, the interaction vessel was sealed during the experiments. As the interaction between the water and the melt begins, steam is generated in the interaction vessel. Based on the pressure history in Fig. 3, the pressure in the interaction vessel will increase continuously, reducing the difference between injection pressure and in-vessel pressure. For the non-explosion case, the pressure in the melt pool increased to approximately 0.17 MPa in 1 s; that is, the injection pressure difference was reduced to approximately 0.18 MPa (initially approximately 0.25 MPa). Although it is not possible to accurately judge when water is injected, considering the experimental conditions of this study, the reduced pressure difference may also be a potential contributing factor to the limited pressure wave intensity. As water is injected into melt pool continuously, pressure difference decreases during water–melt interaction, resulting in lower jet velocity, which signifies that less water enters the melt pool per unit time. From the above analysis, the promoting effect of increasing the injection duration on the injected water volume was limited. Thus, the pressure wave intensity in the melt pool revealed a saturation tendency.

3.2.5 Nozzle diameter

The influence of the nozzle diameter on the pressure build-up characteristics under different melt temperatures (573–673 K) and injection durations (1 s and 2 s) is shown in Fig. 10.

As depicted in Fig. 10, under relatively lower melt-pool temperatures (573–623 K), the pressure wave intensities for nozzle diameters of 2 mm and 4 mm at 1 s injection duration along with 2-mm nozzle diameter at 2 s injection duration were limited in a narrow range. Thus, the promotion effect of increasing nozzle diameter on pressure wave intensity was quite limited under such melt-pool temperature range. By contrast, with a further increase in the temperature in the melt pool, the pressure wave intensity was significantly enhanced to several times that of the previous ones. In general, increasing the nozzle diameter enhanced the pressure wave intensity.

In terms of geometry, doubling the nozzle diameter quadrupled the nozzle exit area. However, under the same injection pressure, the outlet velocity of the jet remained unchanged. Therefore, the flow rate of the 4-mm nozzle was four times larger than that of the 2-mm nozzle; that is, a considerably larger volume of water was injected into the melt pool within the same duration. Consequently,

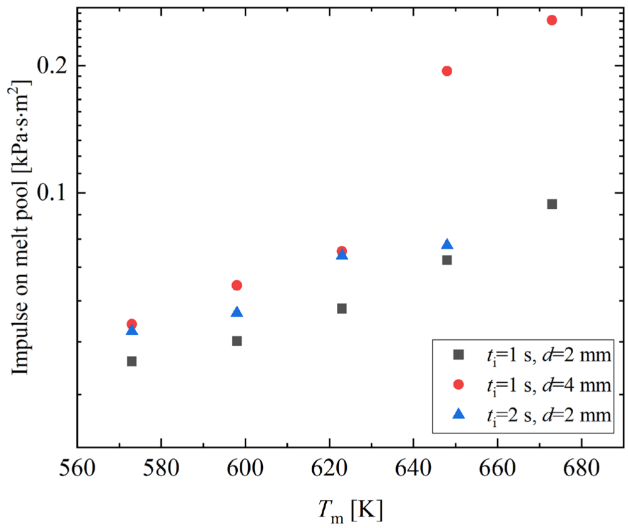

Fig. 10 Influence of nozzle diameter on pressure build-up characteristics (P_i = 0.25 MPa, T_w = 293 K)

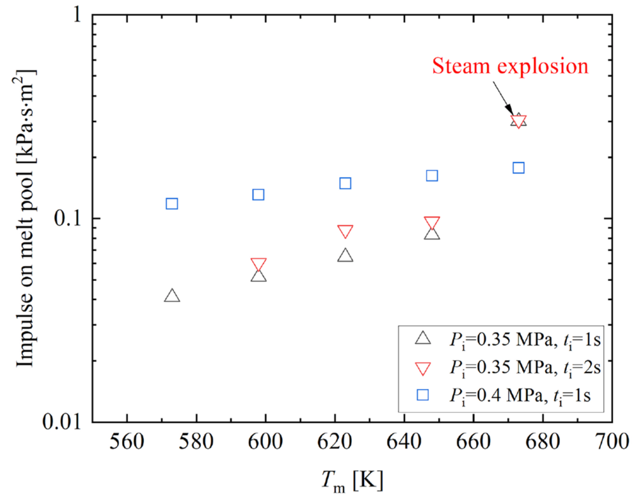

Fig. 11 Influence of interaction mechanism on pressure build-up characteristics (T_w = 293 K, T_m = 673 K, d = 2 mm)

it is not difficult to explain the more intensive pressure wave at higher melt-pool temperatures. Based on previous studies [20–23], the saturation phenomenon of the pressure wave intensity (as the water volume increases) was universally observed regardless of the melt-pool temperature; thus, there is another factor that may lead to such an unusual phenomenon at lower melt-pool temperatures. Based on the flow pattern of the water jet in the melt pool observed previously [10, 11], the water jet was initially in the shape of a cylinder under the effect of inertia with its diameter proportional to the nozzle diameter, pushing away the surrounding melt and creating a cavity. Then, the surrounding melt returned and interacted with the water jet, and the heat transfer occurred mainly in the radial direction. In addition, heat transfer from the melt to the water was relatively less efficient at low melt temperatures, and evaporation and condensation may occur simultaneously in the outer layer of the water jet. Therefore, for a water jet from a nozzle with a larger diameter, only a limited quantity of water was involved in the water–melt interaction under low melt-pool temperatures despite the larger water volume. In contrast, for high melt-pool temperatures, the heat transfer was sufficiently efficient to allow a more complete interaction between the water and melt. Consequently, the pressure wave intensity in the experimental groups with larger-diameter nozzles was limited to low melt-pool temperature conditions.

3.2.6 Interaction mechanism

In addition to the experimental parameters analyzed above, it was found that the interaction mechanism (steam explosion or non-explosion) between water and molten LBE could also influence the pressure build-up characteristics. The influence of the interaction mechanism on the pressure build-up characteristics is shown in Fig. 11, where two group of experimental cases with steam explosion are compared with a higher injection pressure reference group.

3.3 Mechanical energy conversion efficiency

Regardless of the interaction mechanism (steam explosion or non-explosion), the thermal energy of water is partially converted into the mechanical energy of the generated steam and surrounding melt during violent evaporation. Owing to the short interaction duration, such a release of mechanical energy can cause an intensive sloshing motion of the melt pool, posing potential risks to reactor structures. Therefore, it is essential to investigate the mechanical energy conversion efficiency during water–melt interactions.

Based on previous studies [20, 34], the total mechanical energy released during the interaction can be divided into two parts: the compression work of the cover gas (E_c) and the kinetic energy of the melt (E_k). Considering the extremely small scale of the interaction time, an adiabatic process was assumed for the calculation [32]

$$E_c = -\int_{V_0}^{V_1} P\mathrm{d}V = -\int_{V_0}^{V_1} P_0\left(\frac{V_0}{V}\right)^{\gamma}\mathrm{d}V = \frac{P_0V_0}{\gamma-1}\left[\left(\frac{P_1}{P_0}\right)^{\frac{\gamma-1}{\gamma}}-1\right], \tag{5}$$

where P_0 and P_1 are the initial and maximum pressures of the cover gas, respectively, V_0 and V_1 are the volumes of the cover gas corresponding to P_0 and P_1, respectively, and γ is the ratio of the specific heat of the cover gas. Notably, here (and in the following equations), the energy is calculated using the maximum pressure in the cover gas region instead of the terminal pressure. It is frequently observed in the experiments that the pressure in the cover gas region reaches its maximum value and then decreases slightly. The most probable reason for this is that part of the steam may be condensed in the relatively low-temperature upper region of the interaction vessel. Therefore, the energy is underestimated if calculated using the terminal pressure.

By creating 1D acceleration of the inertial mass, the kinetic energy of the melt can be evaluated as [34, 35]:

$$E_k = \frac{I^2}{2m_{pl}}, \tag{6}$$

where m_{pl} denotes the total mass of the melt pool;

The thermal energy consumed during the water–melt interaction (E_{ther}) can be evaluated by calculating the maximum thermal energy absorbable by water:

$$E_{ther} = m_s\left[c_l(T_{sat}-T_w)+h_{fg}+c_g(T_m-T_{sat})\right], \tag{7}$$

where c_l and c_g are the specific heats of liquid water and vapor, respectively, h_{fg} is the latent heat of water, T_{sat}, T_w and T_m are the temperatures of the saturated water, initial water, and melt pool, respectively, and m_s is the total mass of the generated steam, which can be estimated from the pressure variation in the cover gas region [20, 22]:

$$m_s = n_sM_s = M_s\left(\frac{P_1V_{cg}}{RT_1}-\frac{P_0V_{cg}}{RT_0}\right) = (P_1-P_0)M_s\frac{V_{cg}}{RT_1}, \tag{8}$$

where n_s and M_s are the molar quantity and molecular weight of the steam, respectively, V_{cg} is the volume of the cover gas region, R is the gas constant (R=8.314 J/mol/K), and T_1 and T_0 are the cover gas temperatures corresponding to P_1 and P_0. Under the current experimental conditions at the PMCI facility, T_1 and T_0 are almost identical (as shown in Figs. 3 and 4) due to the relatively small volume of water.

By combining Eqs. (4)–(8), the mechanical energy conversion efficiency (η_{TM}) and kinetic energy conversion efficiency of the melt (η_k) during the water–melt interaction can be estimated as follows:

$$\eta_{TM} = \frac{E_c+E_k}{E_{ther}}, \tag{9}$$

$$\eta_k = \frac{E_k}{E_{ther}}. \tag{10}$$

As shown in Fig. 12a, the mechanical and kinetic energy conversion efficiencies of the melt in this study were limited within the ranges of 2.8–4.1% and 0.013–0.7%, respectively. By observing the orders of magnitude of these conversion efficiencies, it was discovered that the mechanical energy release was only an extremely small fraction of the total

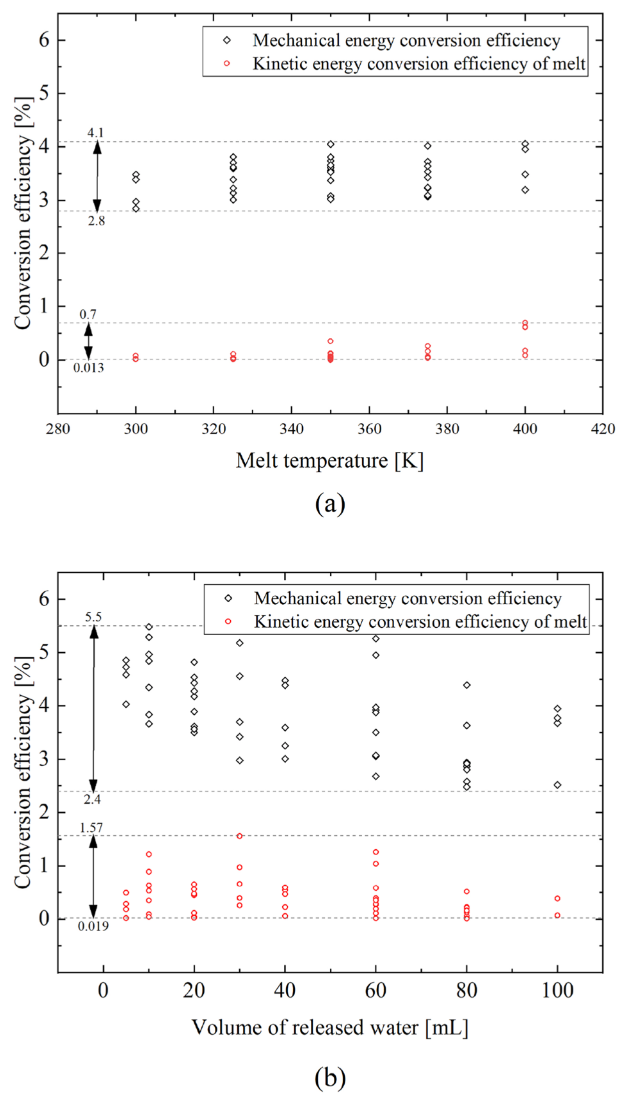

Fig. 12 Conversion efficiency during water–melt interaction. (a) Present water-jet injection mode; (b) Previous water-droplet injection mode [22]

variation in thermal energy. Similarly, the kinetic energy of the melt accounted for only a small fraction of the total release of mechanical energy, signifying that the kinetic energy of the melt was considerably lower than that of the cover gas.

To clarify the effect of the water injection mode, the conversion efficiency of the water-droplet injection mode from a previous study [22] is shown in Fig. 12b as a reference. Through comparison, although the range of the mechanical energy conversion efficiency of the present water jet injection mode had a lower upper limit, no significant difference was observed in terms of the mechanical energy and kinetic energy conversion efficiencies of the melt for these two water–melt interaction modes.

4 Concluding remarks

During an SGTR accident involving an LFR, secondary subcooled pressurized water is injected into the primary melt pool, causing intensive water–melt interactions. Such interactions can result in several complex thermohydraulic phenomena, including flashing of water, sloshing of the melt pool, steam explosion, and vapor bubble transport. Therefore, it is crucial to clarify the mechanisms of the water–melt interaction to acquire a comprehensive understanding of an LFR SGTR accident. In this study, aimed at the first stage of SGTR accident wherein a water jet is injected into the melt pool, several experiments were conducted by injecting pressurized water into a molten LBE pool considering various experimental parameters (melt temperature, water subcooling, injection pressure, injection duration, and nozzle diameter). Through detailed analyses of the pressure build-up characteristics in each experimental case, we found the following:

1. Compared with the water-droplet injection mode, the transient pressure and temperature variations during water–melt interaction exhibited a consistent pattern. Typically a two-phase pressure was observed during pressure build-up.
2. Among the non-explosion cases under current experimental conditions, increasing injection pressure, melt-pool temperature, nozzle diameter, and water subcooling could eventually result in intensified pressure build-up in melt pool.
3. Only a limited enhancement effect on pressure wave intensity was achieved by increasing injection duration. There may be two possible assumptions for this. The generated steam may form a cavity around the jet, which may inhibit the direct contact of water and melt. Alternatively, the continually rising pressure in the interaction vessel may decrease the velocity of water jet.
4. Steam explosion is more likely to occur under certain specific initial water–melt temperature conditions, which could facilitate a more intensive pressure build-up in the melt pool. The instantaneous contact interface temperature was the decisive factor for such initial water–melt temperature conditions.
5. Regardless of the interaction mode (steam explosion or non-explosion), the calculated mechanical and kinetic energy conversion efficiencies of the melt were relatively small (not exceeding 4.1% and 0.7%, respectively). Further, the range of conversion efficiency was similar to previous water-droplet mode, although the upper limit of jet injection mode was slightly lower.

Owing to the invisibility of the interaction process in the PMCI facility, there are still certain uncertainties underlying the water–melt interaction mechanism, particularly the mechanism of saturated pressure build-up while increasing the injection duration. To further contribute to the investigation of LFR SGTR accidents, numerical studies that aim to ascertain the interaction mechanism are highly anticipated in the future. Furthermore, following the international trend of using pure lead as the primary coolant, similar experiments with molten lead may be initiated to enrich the experimental database and improve the availability of current theoretical explanations.

Author contributions All authors contributed to the study conception and design. Material preparation, data collection, and analysis were performed by Hao-Ran Huang, Zi-Jian Deng, Song-Bai Cheng, and Jia-Yue Chen. The first draft of the manuscript was written by Hao-Ran Huang and all authors commented on previous versions of the manuscript. All authors read and approved the final manuscript.

Data availability The data that support the findings of this study are openly available in Science Data Bank at https://cstr.cn/31253.11.sciencedb.j00186.00230 and https://www.doi.org/10.57760/sciencedb.j00186.00230.

Declarations

Conflict of interest The authors declare that they have no conflict of interest.

References

1. OECD/NEA & GIF, Technology Roadmap Update for Generation IV Nuclear Energy Systems (2014)
2. K. Tuček, J. Carlsson, H. Wider, Comparison of sodium and lead-cooled fast reactors regarding reactor physics aspects, severe safety and economical issues. Nucl. Eng. Des. **236**(14–6), 1589–1598 (2006). https://doi.org/10.1016/j.nucengdes.2006.04.019
3. N. Li, Lead-alloy coolant technology and materials—technology readiness level evaluation. Prog. Nucl. Energy **50**(2–6), 140–151 (2008). https://doi.org/10.1016/j.pnucene.2007.10.016
4. I.L. Pioro (ed.), *Handbook of generation IV nuclear reactors* (Woodhead Publishing, Duxford, 2016)

5. W. Huang, D. Zhou, R. Sa et al., Experimental study on thermal-hydraulic behavior of LBE and water interface. Prog. Nucl. Energy. **99**(8), 1–10 (2017). https://doi.org/10.1016/j.pnucene.2017.04.005
6. T.N. Dinh, Multiphase flow phenomena of steam generator tube rupture in a lead-cooled reactor system: a scoping analysis. In: Proceedings of ICAPP 2007, Nice, France (2007)
7. A.S. Iskhakov, V.I. Melikhov, O.I. Melikhov et al., Steam generator tube rupture in lead-cooled fast reactors: estimation of impact on neighboring tubes. Nucl. Eng. Des. **341**, 198–208 (2019). https://doi.org/10.1016/j.nucengdes.2018.11.001
8. A.S. Iskhakov, V.I. Melikhov, O.I. Melikhov et al., Hugoniot analysis of energetic molten lead-water interaction. Ann. Nucl. Energy. **129**, 437–449 (2019). https://doi.org/10.1016/j.anucene.2019.02.018
9. A.V. Beznosov, S.S. Pinaev, D.V. Davydov et al., Experimental studies of the characteristics of contact heat exchange between lead coolant and the working body. Atom. Energy. **98**(3), 170–176 (2005). https://doi.org/10.1007/s10512-005-0188-4
10. Y. Sibamoto, Y. Kukita, H. Nakamura, Visualization and measurement of subcooled water Jet injection into high-temperature melt by using high-frame-rate neutron radiography. J. Nucl. Sci. Technol. **139**, 205–220 (2002). https://doi.org/10.13182/NT02-A3314
11. Y. Sibamoto, Y. Kukita, H. Nakamura, Small-scale experiment on subcooled water jet injection into molten alloy by using fluid temperature-phase coupled measurement and visualization. J. Nucl. Sci. Technol. **44**(8), 1059–1069 (2007). https://doi.org/10.1080/18811248.2007.9711347
12. C. Zhang, R. Sa, D. Zhou et al., Effects of gas velocity and break size on steam penetration depth using gas jet into water similarity experiments. Prog. Nucl. Energy **98**, 38–44 (2017). https://doi.org/10.1016/j.pnucene.2017.02.006
13. H. Cheng, S. Chen, H. Huang et al., Study on water jet penetration behavior in molten LBE during SGTR accident with simulant experiments. Nucl. Eng. Des. **411**, 112413 (2023). https://doi.org/10.1016/j.nucengdes.2023.112413
14. A. Ciampichetti, D. Pellini, P. Agostini et al., Experimental and computational investigation of LBE-water interaction in LIFUS 5 facility. Nucl. Eng. Des. **239**(11), 2468–2478 (2009). https://doi.org/10.1016/j.nucengdes.2009.08.007
15. A. Ciampichetti, D. Bernardi, T. Cadiou et al., LBE-water interaction in LIFUS 5 facility under different operating conditions. J. Nucl. Mater. **415**(3), 449–459 (2011). https://doi.org/10.1016/j.jnucmat.2011.04.051
16. Q. Yu, Y. Fang, Y. Zhao et al., Experimental investigation of pressure fluctuation and steam transport under SGTR accident in Lead-cooled Fast Reactors. I. J. Heat. Mass. Tran. **207**, 12388 (2023). https://doi.org/10.1016/j.ijheatmasstransfer.2023.123988
17. A. Pesetti, A. Del Nevo, N. Forgione, Experimental investigation and SIMMER-III code modelling of LBE-water interaction in LIFUS5/Mod2 facility. Nucl. Eng. Des. **290**, 119–126 (2015). https://doi.org/10.1016/j.nucengdes.2014.11.016
18. X. Huang, P. Chen, Y. Yin et al., Numerical investigation on LBE-water interaction for heavy liquid metal cooled fast reactors. Nucl. Eng. Des. **361**, 110567 (2020). https://doi.org/10.1016/j.nucengdes.2020.110567
19. S. Cheng, K. Matsuba, M. Isozaki et al., An experimental study on local fuel-coolant interactions by delivering water into a simulated molten fuel pool. Nucl. Eng. Des. **275**, 133–141 (2014). https://doi.org/10.1016/j.nucengdes.2014.05.003
20. S. Cheng, T. Zhang, C. Meng et al., A comparative study on local fuel-coolant interactions in a liquid pool with different interaction modes. Ann. Nucl. Energy **132**, 258–270 (2019). https://doi.org/10.1016/j.anucene.2019.04.048
21. S. Cheng, Y. Dong, X. Chen et al., Experimental study on local fuel-coolant interaction in molten pool with different melts. Ann. Nucl. Energy **149**, 107760 (2020). https://doi.org/10.1016/j.anucene.2020.107760
22. S. Cheng, Y. Zou, Y. Dong et al., Experimental study on pressurization characteristics of a water droplet entrapped in molten LBE pool. Nucl. Eng. Des. **378**, 111192 (2021). https://doi.org/10.1016/j.nucengdes.2021.111192
23. T. Zhang, S. Cheng, T. Zhu et al., A new experimental investigation on local fuel-coolant interaction in a molten pool. Ann. Nucl. Energy **120**, 593–603 (2018). https://doi.org/10.1016/j.anucene.2018.06.031
24. S. Cheng, K. Matsuba, M. Isozaki et al., A numerical study on local fuel-coolant interactions in a simulated molten fuel pool using the SIMMER-III code. Ann. Nucl. Energy **85**, 740–752 (2015). https://doi.org/10.1016/j.anucene.2015.06.030
25. S. Yan, J. Wan, F. Zhao et al., Modeling and control simulation of the China CLEAR-IB. Annl. Nucl. Energy **68**, 53–60 (2014). https://doi.org/10.1016/j.anucene.2014.01.019
26. W. Huang, R. Sa, Q. Huang et al., Experimental study on fragmentation behaviors of molten LBE and water contact interface. Nucl. Sci. Tech. **26**, 060601 (2015). https://doi.org/10.13538/j.1001-8042/nst.26.060601
27. Z. Deng, S. Cheng, H. Cheng, Experimental investigation on pressure-buildup characteristics of a water lump immerged in a molten lead pool. Nucl. Sci. Tech. **34**(3), 35 (2023). https://doi.org/10.1007/s41365-023-01188-1
28. T.A. Dullforce, D.J. Buchanan, R.S. Peckover, Self-triggering of small-scale fuel-coolant interactions. J. Phys. D Appl. Phys. **9**, 1295–1303 (1976). https://doi.org/10.1088/0022-3727/9/9/006
29. S. Kondo, K. Konishi, M. Isozaki et al., Experimental study on simulated molten jet-coolant interactions. Nucl. Eng. Des. **155**, 73–84 (1995). https://doi.org/10.1016/0029-5493(94)00870-5
30. A. Simons, I. Bellemans, T. Crivits et al., Heat transfer considerations on the spontaneous triggering of vapor explosions-a review. Metals **11**(1), 55 (2021). https://doi.org/10.3390/met11010055
31. H.K. Fauske, On the mechanism of uranium dioxide-sodium explosive interactions. Nucl. Sci. Eng. **51**, 95–101 (1973). https://doi.org/10.13182/NSE73-A26584
32. J.H. Lienhard, Correlation for the limiting liquid superheat. Chem. Eng. Sci. **31**, 847–849 (1976). https://doi.org/10.1016/0009-2509(76)80063-2
33. V.K. Dhir, G.P. Purohit, Subcooled film-boiling heat transfer from spheres. Nucl. Eng. Des. **47**(1), 49–66 (1978). https://doi.org/10.1016/0029-5493(78)90004-3
34. T. Tsuruta, M. Ochiai, S. Saito, Fuel fragmentation and mechanical energy conversion ratio at rapid deposition of high energy in LWR fuels. J. Nucl. Sci. Technol. **22**(9), 742–754 (1985). https://doi.org/10.1080/18811248.1985.9735721
35. J.H. Kim, B.T. Min, I.K. Park et al., Triggered steam explosions with the corium melts of various compositions in a two-dimensional interaction vessel in the TROI facility. Nucl. Technol. **176**(3), 372–386 (2010). https://doi.org/10.13182/NT11-A13314